MULTI-MODAL GEOSPATIAL AND THEMATIC DATA TO FOSTER GREEN DEAL APPLICATIONS

R. Beber[1], G. Perda[1], N. Takhtkeshha[1], F. Remondino[1], T. Maffei[2], D. Poli[2], K. Moe[3], P. Cipriano[4], M. Ciliberti[4]

[1] 3D Optical Metrology (3DOM) unit, Bruno Kessler Foundation (FBK), Trento, Italy
– Email: <rbeber><gperda><ntakhtkeshha><remondino>@fbk.eu
[2] AVT Airborne Sensing Italia srl, Trento, Italy – Email: <t.maffei><d.poli>@avt.at
[3] Vermessung AVT-ZT-GmbH, Imst, Austria – Email: k.moe@avt.at
[4] Deda Next, Italy – Email: <Piergiorgio.Cipriano>< Marika.Ciliberti>@dedagroup.it

Commission I

KEY WORDS: Photogrammetry, LiDAR, hyperspectral, thermal, mapping, 3D, dataset, Green Deal, climate change

ABSTRACT:
The Urban Data Space for Green Deal - USAGE - project is founded by the European Union (EU) to support the green transition of cities. Within USAGE, a series of geospatial, thematic and other datasets have been newly acquired or created to test and evaluate solutions (i) to better understand issues and trends on how our planet and its climate are changing and (ii) to address the role that humans play in these changes, e.g., with behaviour adaptation and mitigation actions. The paper aims to provide some relevant datasets collected in two urban areas, reporting processing methodologies and applications of analysis-ready and decision-ready geospatial data. The shared data are unique urban datasets due to their resolutions and sensors type and could boost progresses of geospatial procedures to create and use data useful for climate change adaptation, renewable energy monitoring and management, etc.

Figure 1. Possible analysis- and decision-ready geospatial products useful to support the green transition of cities: semantically-enriched point clouds (a), building footprints extracted from orthoimage (b), aerial thermal image (c) and surface material classification map from aerial hyperspectral images (d).

1. INTRODUCTION

The European Union (EU) is pushing for the creation of a European single market for data which promotes, within a horizontal data sharing legislation, the cross-sector sharing of data, to facilitate innovative solutions and support the decarbonization of the energy system. To do so, Findability, Accessibility, Interoperability and Reuse (FAIR[1]) principles must be adopted and, in this contest, different projects aiming at the creation of Green Deal data space (Gutierrez David et al., 2023) have been funded to support the green transition of cities (Amado and Poggi, 2022).
The Urban Data Space for Green Deal - USAGE[2] - EU project is one of them. Within USAGE, a series of geospatial, thematic and other datasets have been newly acquired or created in order to test and evaluate solutions for urban data spaces (i) to better understand issues and trends on how our planet and its climate are changing (Rüegg, 2019), and (ii) to address the role that humans play in these changes, e.g. with behavior adaptation and mitigation actions (Foshag et al., 2020). As cities are the largest consumer of energy resources (Gago et al., 2013) and are more vulnerable than other areas to climate changes (Wouters et al., 2019), solutions in USAGE are found by meeting multiple and diverse requirements. These solutions are developed on the basis of inter- and transdisciplinary cooperation, analysing geospatial data and incorporating local knowledge (Adler et al., 2018). Public authorities, city planners and all urban actors willing to participate to green transitions, need to be equipped with simple but operative ICT tools, geospatial solution, strategies and methodologies for proper energy monitoring and management, renewable energy usage and climate change adaptation (Nowacka and Remondino, 2018).

1.1 Paper's contribution

The paper aims to provide to the scientific community some relevant geospatial datasets and products (Figure 1) that were collected within the USAGE project in two of its four pilot areas (Ferrara, Italy and Graz, Austria). The provision of these data in support of policy and decision makers has two main aims:

- to develop, test and validate geospatial procedures to derive 2D/3D geospatial data (semantically enriched point clouds, 3D building models, etc.) later in the paper called analysis-ready geospatial data;
- to develop, test and validate solutions to derive thematic products (maps of Urban Heat Islands, distribution of photovoltaic potential of buildings, customized classification maps, etc.) later in the paper called decision-ready geospatial data.

2. THE USAGE DATASET AND RELATED WORKS

Due to the focus of the USAGE project, the datasets[3] (Table 1) are strongly related to the urban environment. Data are mainly

[1] https://www.go-fair.org/fair-principles/
[2] https://www.usage-project.eu/
[3] https://github.com/3DOM-FBK/USAGE_Geospatial

Datasets	***Ferrara, Italy***		***Graz, Austria***	
	Resolution and sensor specs	**Year**	**GSD resolution / specs [sensor]**	**Year**
Aerial images (nadir)	10 cm, RGBI bands, [Vexel UltraCam Osprey 4.1]	2022	10 cm, RGBI bands, [Vexcel UltraCam Osprey 4.1]	2022
Aerial images (oblique)	n.a.	-	ca 9-13 cm, RGB bands, [Vexcel UltraCam Osprey 4.1]	2022
Orthophotos	10 cm, RGBI bands	2022	10 cm, RGBI bands	2022
LIDAR point cloud	10 pt m^2 [Riegl VQ780ii]	2022	4 pt m^2 [Riegl VQ780ii]	2022
DTM, DSM	1 m raster grid	2022	0.5m raster grid	2022
Hyperspectral images	1 m, 364 bands, VNIR and SWIR (0,4 - 2,5 µm) [AisaFENIX384 by Specim]	2022	1.8 m, 364 bands, VNIR and SWIR (0,4 - 2,5 µm) [AisaFENIX384 by Specim]	2021
Thermal images	1m, night, LWIR (7,5 - 14,0 µm) [DualDigiTHERM by IGI]	2023	0.5 m, day and night, LWIR (7,5 - 14,0 µm) [DualDigiTHERM by IGI]	2021
Sentinel 3- SLSTR	1.4 km MWIR & LWIR	2018 -	*as for Ferrara*	
Landsat 8 & 9	30 m (VIS, NIR, SWIR)	2013 -	*as for Ferrara*	
Land cover	1 m grid	2022	1.8 m grid	2021
Building footprints	Vector layer, based on cadastre	2022	Vector layer, based on cadastre	2021
Weather Stations data	T_2m, rainfall, RH, wind_dir & _mag	2000	*as for Ferrara*	2000

Table 1: The geospatial and thematic USAGE datasets over the cities of Ferrara (Italy) and Graz (Austria).

kept on the open data portal of each city in their national language and, for easy accessibility, stored in the project repository. Beside "pure" geospatial and thematic data, also environmental time series measurements from ground weather stations are reported.
With respect to the available geospatial datasets (Rottensteiner et al., 2012; Xia et al., 2017; Özdemir et al., 2019; Garcia-Moreno et al., 2020; Hong et al., 2021; Kölle et al., 2021), USAGE features the following unique characteristics:

- imagery with different spectral ranges (VNIR, SWIR, LWIR);
- spectral and geometric high-resolution imagery (geometric resolution up to 10 cm / pixel, spectral resolution up to 5 nm / channel);
- multi-sensor data (optical sensors, LiDAR sensors, ground stations, etc.);
- heterogeneous topography (flat and hilly urban areas);
- 2D and 3D geospatial and thematic data.

The aim of the collected datasets is to foster and motivate geospatial research activities related to data processing and added-value information extraction (analysis-ready and decision-ready geospatial data). This includes:

- aerial image triangulation with learning-based features (Remondino et al., 2022);
- co-registration of multi-modal and multi-spectral images (Ruiz de Ona et al., 2023);
- co-registration of LiDAR and optical data (Toschi et al., 2021);
- evaluate production pipeline solutions for large-scale mapping purposes (Moe et al., 2016; Toschi et al., 2017);
- evaluation of conventional or learning-based MVS / dense image matching methods (Chebbi et al., 2023; Liu et al., 2023; Stathopoulou and Remondino, 2023);
- NeRF-based 3D reconstruction (Turki et al., 2022; Remondino et al., 2023;);
- automatic radiometric correction of large-size orthophotos (Lelégard et al. 2022).

Furthermore, the datasets could be valuable for the realization and validation of algorithms for the generation of other (geo)products to support Green Deal policies, such as:

- image classification for large scale map generation (Shi et al., 2019; Minaee et al., 2021);
- data fusion (Hu et al., 2023);
- semantic segmentation of point clouds (Koelle et al., 2021; Özdemir et al., 2021; Grilli et al., 2023);
- analysis of thermal images (Gerhards et al., 2018);
- building footprint extraction from point clouds (Wu et al., 2018; Buyukdemircioglu et al., 2022);
- 3D building/city model generation (Lafarge and Mallet., 2012; Biljecki et al., 2015; Özdemir and Remondino, 2018);
- photovoltaic potential estimation of building roof or other suitable areas (Nex et al., 2013; Giannelli et al., 2022);
- urban heat island analysis and forecasting (Voelkel and Shandas, 2017; Bosch et al., 2021; Ellena et al., 2023);
- urban tree mapping using hyperspectral and LiDAR data fusion (Dalponte et al., 2013; Ballanti et al., 2020);
- derivation of urban ecological indexes (Darvishzadeh et al., 2009; Heiden et al., 2012; Sun et al., 2021).

3. ANALYSIS-READY GEOSPATIAL DATA

In the Earth Observation (EO) community, raw data coming from sensors are subsequently processed up to levels that allow end-users to directly apply certain workflows in a homogenized fashion. For this reason, the term *analysis-ready* is adopted to categorize this type of processed data. In the following sections the most common analysis-ready data are described.

3.1 Dense point clouds from oblique aerial images

Multiview stereo matching (MVS) can produce detailed and accurate 3D models of urban environments, including buildings, streets and infrastructure. The Graz oblique dataset, flown by AVT in September 2022 with UltraCam Osprey 4.1 camera, was used to prove the benefits of oblique imagery for detailed urban modeling. In the area of the University of Graz headquarters two sub-blocks of images were chosen: the first one containing just 11 nadir images, the second containing 61 oblique plus the 11 nadir images. After running the aerial triangulation, two dense point clouds were generated on the two datasets with grid equal to 2 x GSD, resulting in a point density higher than 25 pts/sqm. Figure 2 shows some zooms on the two point clouds that reveal the advantage of using nadir and oblique datasets, with respect to the nadir-only one. Indeed, the point clouds achieve richer content, unveiling objects such as building facades and footprints in narrow streets. Nevertheless, this comes at the cost of higher object occlusion, significant differences in object scales and illuminations and sudden depth variations, all still open issues to achieve accurate 3D reconstructions (Rupnik et al., 2014). The final analysis-ready Graz point cloud covers an area of approximately 11 sqkm and contains some 1.6 billion points.

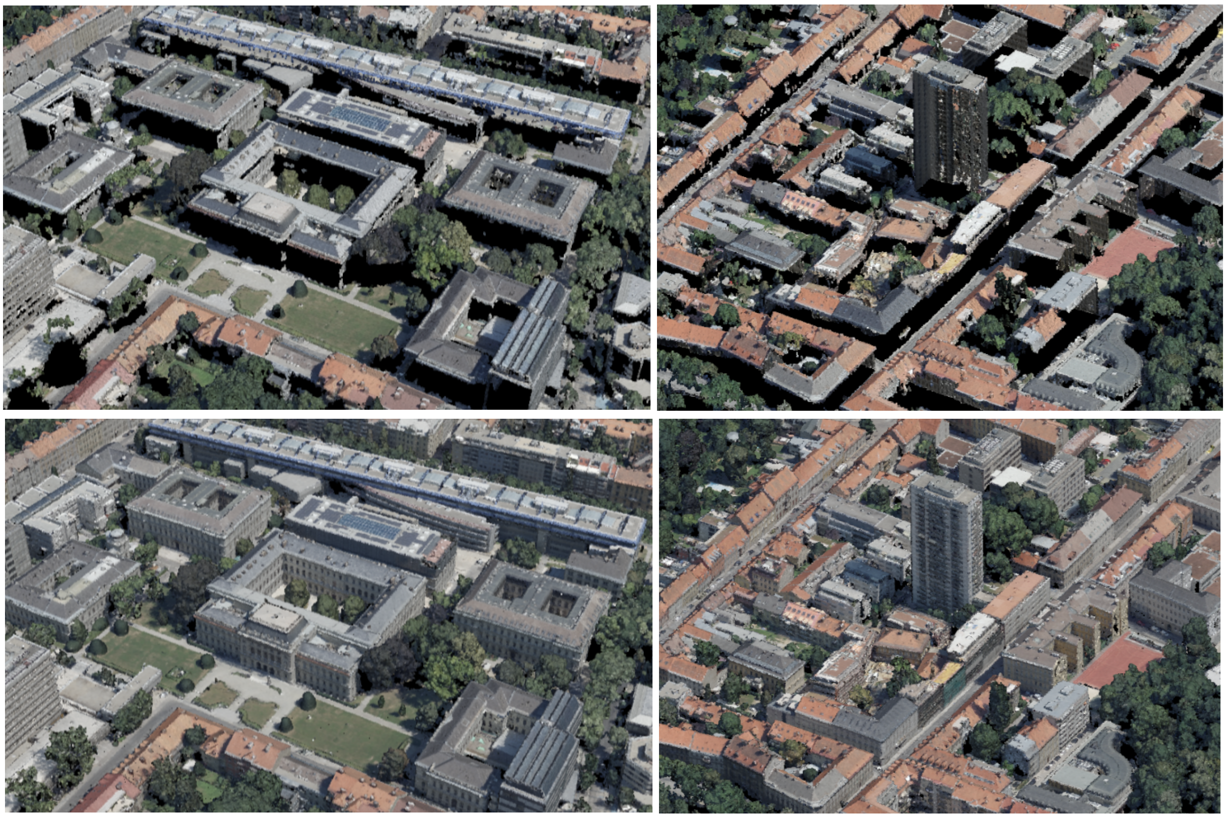

Figure 2. Dense point cloud created with only aerial nadir images (top) and with aerial nadir & obliques (bottom). Holes on the facades are present when oblique images are not included in the MVS processing.

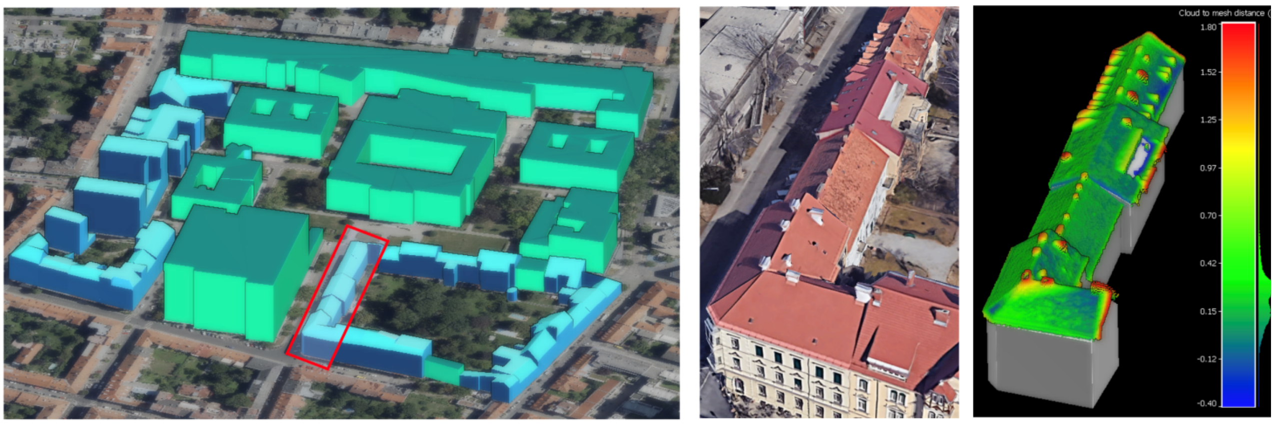

Figure 3. Results of 3D building generation: LOD1 (green) and LOD2 (blue) models overlaid on orthophoto (left). Mesh model of the highlighted building block (centre). Fitting error as distance between the LOD2 buildings and the input DSM cloud (right).

The quality of the dense point cloud is crucial when the point cloud itself acts as input for further (3D) processes, as any shortcomings in its quality will have an impact on subsequent results. For example, without oblique imagery the 3D reconstruction of building facades, thus the estimation of solar potential on them, would be incomplete. Poor quality and sparse point clouds on roofs would miss important details to accurately estimate the solar potential and would also reflect on the quality of derived standard photogrammetry products such as DTM, DSM and true-orthophotos.

3.2 Building models

3D representations of the urban environment are normally denoted with levels of detail (LOD - Biljecki et al., 2016). Starting from the produced DSM and DTM, the vector layer of building footprints can be extruded to generate LOD1 products. Using the python libraries *shapely* and *mapbox_earcut* and in-house code, *OBJ* or *CityGML* results can be created. On the other hand, LOD2 buildings are generated fitting planes on the available DSM in the areas identified by the vector layer of the footprints. Using C*ity3D* (Huang et al., 2022), different DSM resolutions (10cm, 20cm, 50cm, 1m) are tested: finally, it was noted that too fine resolutions produce wrong fitting results with an exponential processing time and 50 cm is a suitable resolution for standard buildings. Results of LOD1 and LOD2 generation from aerial point clouds are shown in Figure 3.

4. DECISION-READY GEOSPATIAL DATA

Decision-ready geospatial data are here defined as those datasets that, with minor interpretation of associated attributes or statistics, allow end-users to take actions and decisions upon a certain area.

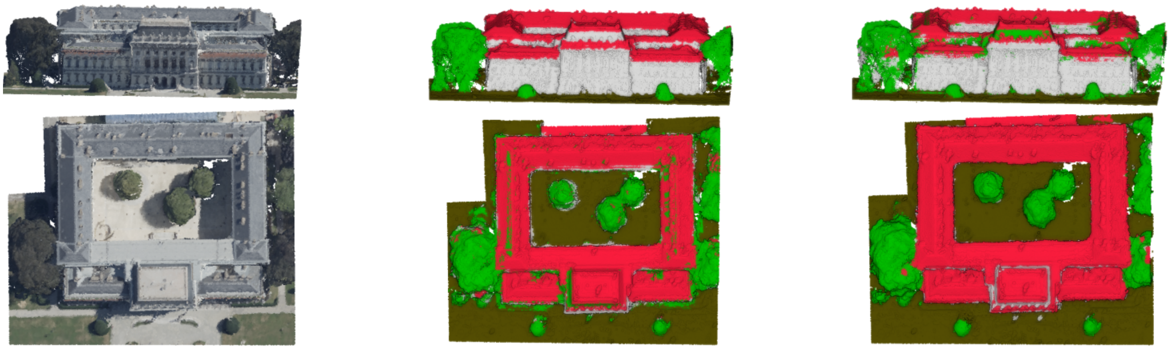

Figure 4. Front and top views of classification results of the University of Graz main building. RGB point cloud (left). RF results revealing inaccuracies in the classes (center); more accurate results with PT (right).

4.1 Semantically enriched 3D point cloud

Two supervised classification algorithms are applied on 3D point clouds: Random Forest (RF - Grilli and Remondino, 2020) and Point Transformer (PT - Zhao et al., 2021). Meaningful geometric features are computed to characterize the pre-defined classes ground, facades, roofs and vegetation. Training and evaluation subsets are then extracted and manually labelled. Both algorithms are run with a selection of significant features at different radii. Worth to mention that sphericity characterizes tree canopies while verticality differentiates between ground and facades. Distance from ground sets flat roofs and ground apart while planarity helps with sloping roofs.

	Ground	Facades	Roofs	Veget.	Avg.
RF-Precision	**87%**	92%	**95%**	71%	86%
PT-Precision	78%	**95%**	87%	**96%**	**89%**
RF-Recall	82%	92%	86%	**80%**	85%
PT-Recall	**95%**	**93%**	**95%**	77%	**89%**
RF-F1 score	84%	92%	90%	75%	85%
PT-F1 score	**86%**	**94%**	**91%**	**85%**	**89%**

Table 1: Metrics of RF and PT classification on Graz.

The two classification methods are compared in terms of per class precision, recall, F1 and their average scores (Table 1). For roof and façade classes, completeness is higher with PT than RF, showing a higher recall score. Although the results are metrically similar, PT performs better visually, returning more homogenous classes (Figure 4). The used classes are propaedeutic to generate other decision-ready data such photovoltaic (PV) potential estimation maps (Section 4.3).

4.2 Urban Heat Island (UHI)

Heat waves are more and more heavily affecting population and this is even more enhanced in urban areas rather than in the countryside. Municipalities need actionable data to support their decisions. UHI can be defined as the temperature difference between urban and rural areas, triggered by the excess of heat emitted and by the solar gain caught by man-made structures. UHI and heat risk maps can be used as forecasting tool but also to support policies, renovations or regulations at municipality level (Di Napoli et al., 2020). UHI maps can be created integrating EO imagery, IoT ground sensor data, surface properties, machine learning and geostatistics. In the developed pipeline a regression is computed amongst the available stations of the area of interest (AOI) and the Land Surface Temperature (LST) derived from Landsat 9 satellite images (Ermida et al., 2020). The coefficients of the regression are then geographically weighted with NDVI, DTM and other auxiliary datasets. The corrected regression coefficients are then spatialized over the AOI through a Kriging method. This allows to correctly spatialize the weather station temperature thanks to the spatially resolute (30 m) information provided by the thermal band of the satellite. A predicted UHI map in Ferrara is shown in Figure 5b: the spatialize temperature (on August 4th 2022) clearly shows the hottest spot within the industrial (upper left) and urban (centre) areas, with also some hot spots in the bare soil that need to be further investigated. If other UHI maps are computed for other days, maps of temperature differences can be generated. Figure 5c (August 4th 2022 vs July 19th 2022) highlights a decrease in temperature in some vegetated fields due to crop growing and an increase in temperature due to accumulation of heat in the historic city centre and in the industrial district. The fields on the top right corner show higher temperature due to the exposure of bare soil after some crop harvesting.

a) 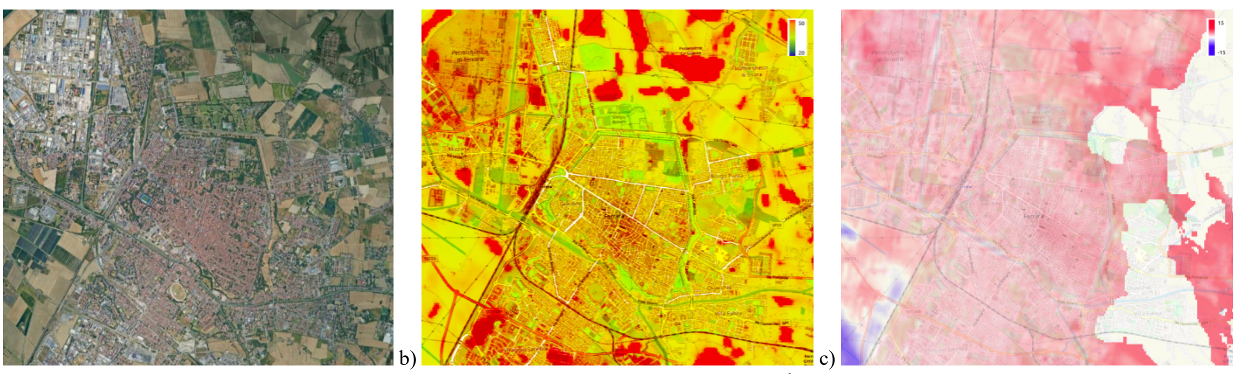

Figure 5. RGB Sentinel 2 image of Ferrara, Italy (a), predicted temperature on Aug 4th, 2022 (b) and temperature difference between Jul 19th and Aug 4th 2022 (c): the missing pixels are due to cloud masking in the pipeline for the 19/07 Landsat 9 acquisition.

4.3 Photovoltaic (PV) potential estimation

PV potential estimation is crucial in the transition of our cities to a greener economy. The USAGE data over Graz are used to compare two methods: a conventional approach based on 2.5D raster data (PV2.5D - Hofierka and Sury, 2002) - limited to rooftops only, and an approach which employs 3D point clouds (VOSTOK[4]), to compute the PV potential of building facades too. Results are validated with respect to the total solar radiation (SR) measured by weather station in the year 2022. The focus is on SR without computing PV potential as the latter depends on physical parameters. Both approaches correct for the atmospheric absorption and scattering of solar radiation under clear sky using the Linke atmospheric turbidity coefficient. PV2.5D uses Linke raster maps while VOSTOK uses a Linke constant factor of 3 which is near the annual average for rural-city areas in Europe. Additionally, PV2.5D considers a correction for ground albedo (set to 0.2). VOSTOK is also used to compute the SR only on roofs. Points belonging to the "roofs" and "façade" classes are extracted from the classified point cloud (Section 4.1).
Figure 6 shows annual results for both approaches. In general, PV2.5D tends to estimate lower values of SR than VOSTOK. Of course, the increase in solar power when including facades is not constant throughout the year, registering a peak gain of 1.4 GWh for the month of July against 0.2 GWh for December. The two approaches were validated by comparing computed SR values with data logged from the University of Graz weather station. An area of about 70 sqm is used for the comparison. Daily SR averages are computed for each approach and the results are plotted together with 14-days moving averages for years 2017 to 2022 as well as the six years period average (Figure 6). VOSTOK estimates higher values than PV2.5D, possibly due to an overestimation of surface area since it uses 3D point clouds. Other minor discrepancies may depend on the absence of the albedo constant in VOSTOK, the choice between constant and variable Linke factors, and the voxel size for shadows casting. The computation time is primarily influenced by raster resolution and AOI size, while VOSTOK computation time depends mainly on the point cloud density.
Values of SR on facades computed with VOSTOK could be integrated with the results of other rooftop PV potential estimation tools such as Google Maps Platform Solar API[5] to provide conclusive insights on solar energy output per building.

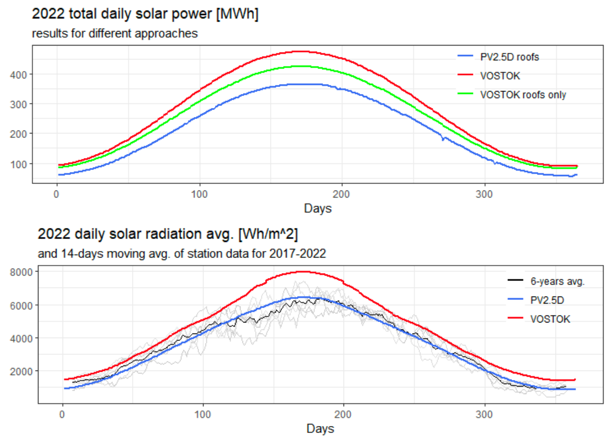

Figure 6: Daily increase of solar radiation when including building facades in the PV computation (top). Solar radiation validation with data from the Graz University weather station and computed averages for the station area for VOSTOK and PV2.5D (bottom).

4.4 Material classification map and urban indices

Ortho-ready hyperspectral images can be used for a variety of analyses with AI-based approaches. The available images over Graz and Ferrara were used to extract information on the ground and roof material types (Figure 1d) using a multi-level machine learning approach, supported by training data provided by the municipalities. The final result of the material classification map of Graz reached an overall accuracy of 93,18% and kappa of 0,9271. Urban, ecological and vegetation indices can also be produced (Figure 7).

4.5 Characterization of vegetated areas

Thematic (i.e., species, biophysical properties) and geometric information (i.e., height, trunk diameter, canopy surface area) on trees in forests or urban areas is essential to monitor health and growth of trees over time, to estimate biomass and to map species distribution. Urban green management currently relies on visual identification and mapping of trees, 2D maps and traditional databases, but it could benefit from 3D digital inventories based

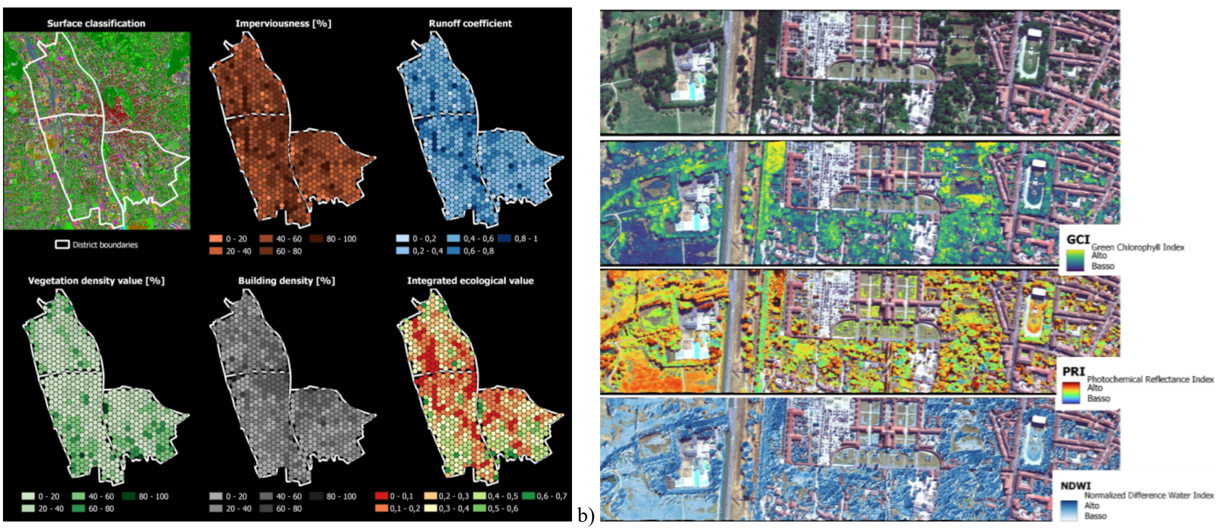

Figure 7. Thematic maps from aerial hyperspectral images: roof and ground materials and ecological indices over Graz dataset (left), vegetation indices over Ferrara (right).

[4] https://github.com/GIScience/vostok

[5] https://developers.google.com/maps/documentation/solar

https://doi.org/10.5194/isprs-archives-XLVIII-1-W3-2023-9-2023

on geospatial data, that are objective, high-resolution, large scale, and accurate. Existing methodologies for tree identification and metric analysis rely on LiDAR (Balsi et al., 2018; Hyyppä et al., 2022) or photogrammetric point clouds (Nevalainen et al., 2017; Carr and Slyder, 2018) while hyperspectral data, either images (Ballanti et al., 2016; Liang et al., 2020) or point clouds (Tian et al., 2022), are necessary for species identification and health status monitoring. Figure 8 show results on point clouds for single tree identification (a) and crown radius (b). Derived queryable maps with single trees or tree species are shown in Figure 8c-d.

4.6 Thermal analyses

Understanding the land surface temperature (LST) and material temperatures in the urban environment is important in numerous application such as UHI, roof heat leakage detection, illicit sewage disposal, vegetation stress estimation, crop yield estimation., etc. Given the USAGE data, a comparison is made between a high-resolution airborne thermal acquisition at 0.5m and the by-weekly availability of Landsat 8&9 thermal data (30m) to understand how representative the second is of the first. Since non-contact measurement of surface temperature heavily rely on material emissivity, the comparison is performed on the material classes derived from hyperspectral acquisition (Section 4.4). Moreover, a direct comparison is made between the two atmospheric corrected dataset with a time lag of 3 days by aggregating the resolute data to 30m using the mode as metric.
In Figure 9a the airborne corrected thermal acquisition over Graz is shown: the urban environment pops out due to the material properties of the surfaces and their high emissivity, revealing sudden differences between the built and rural environment. Figure 9b shows the Landsat acquisition with the major trends of temperature distribution amongst the different land use. Figure 9c reports the temperature difference between the two products. Red areas depict higher LST measured by the airborne sensor compared to the satellite sensor as, thanks to the 0.5 m resolution, buildings are better distinguishable. The blue areas show higher temperatures in the satellite derived LST, that is mostly present in the river. Apparently, the satellite is good in measuring LST in vegetated areas where the two sensors produce similar results. This imply that satellite derived LST is more accurate for urban landscapes rather than in the urban environment.

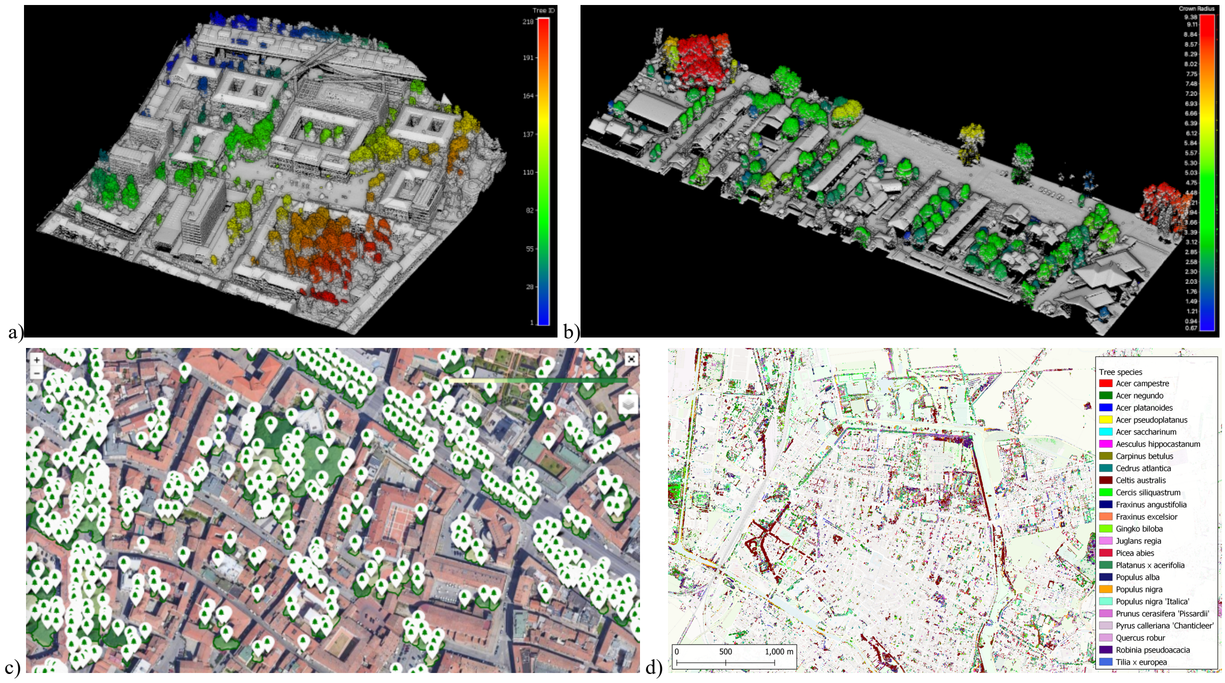

Figure 8. Individual tree segmentation from airborne LiDAR data (a) ad crown radii (b). GIS visualization of canopy maps (c) and tree species mapping from aerial hyperspectral images (d).

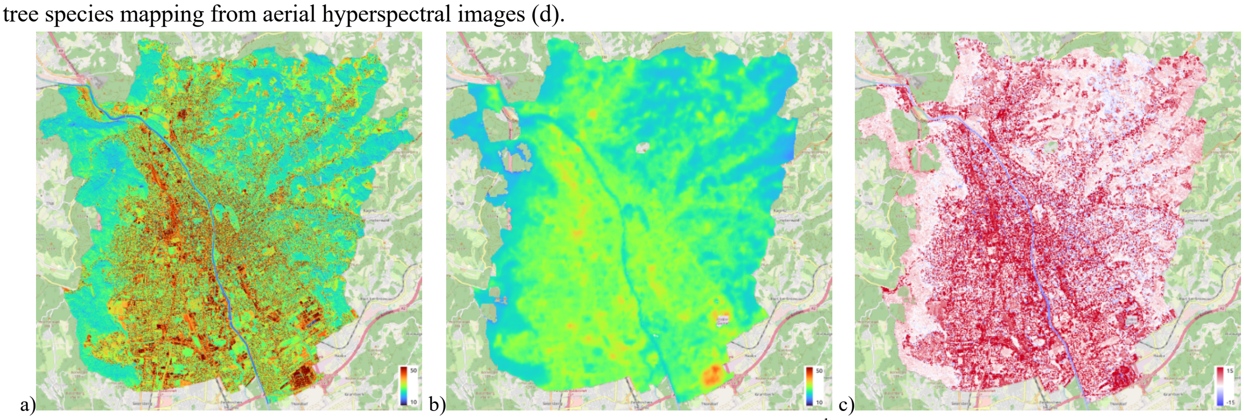

Figure 9. Surface temperature (0.5 m) from aerial thermal images acquired on Sept 9th 2021 (a). Landsat 8 image acquired on Sept 12th 2021 (b). Difference between upscaled (30 m) airborne LST and Landsat 8 LST (30m) (c).

https://doi.org/10.5194/isprs-archives-XLVIII-1-W3-2023-9-2023 |

5. CONCLUSIONS

Europe has planned to become a leader in a data-driven society by launching Green Deal and European data spaces activities in different strategic societal sectors. Data spaces are envisaged as trustworthy FAIR sharing environments where data can be used by multiple interdisciplinary actors. The paper presented the USAGE activities and datasets offered to the R&D community to develop and evaluate geospatial solutions to foster Green Deal applications. Processing methodologies and achievable results are also presented on two pilot areas of the USAGE project. The paper showed how 2D and 3D analysis- and decision-ready products created from geospatial data could support municipalities, decision makers and citizens to plan intervention, heat mitigation approaches or renovations, identify hotspots and vulnerable regions, assess surface materials or canopy information, support sustainable management, etc.

ACKNOWLEDGMENTS

The work is partly funded by the EU project USAGE - Urban Data Space for Green Deal (https://www.usage-project.eu/) which has received funding from the European Union's Horizon Europe Framework Programme for Research and Innovation under the Grant Agreement no 101059950 - call HORIZON-CL6-2021-GOVERNANCE-01-17 (IA).

REFERENCES

Adler, C., Hirsch Hadorn, G., Breu, T., Wiesmann, U., Pohl, C., 2018. Conceptualizing the transfer of knowledge across cases in transdisciplinary research. *Sustainable Science*, 13 (1), pp. 179-190.

Amado, M., Poggi, F., 2022. *Sustainable Energy Transition for Cities*. Elsevier, ISBN 978-0-12-824277-3.

Ballanti, L., Blesius, L., Hines, E. and Kruse, B., 2016. Tree species classification using hyperspectral imagery: A comparison of two classifiers. *Remote Sensing*, 8(6), p.445.

Balsi, M., Esposito, S., Fallavollita, P., & Nardinocchi, C., 2018. Single-tree detection in high-density LiDAR data from UAV-based survey. *European Journal of Remote Sensing*, *51*(1), 679–692.

Biljecki, F., Stoter, J., Ledoux, H., Zlatanova, S., Coltekin, A., 2015. Applications of 3D City Models: State of the Art Review. *ISPRS International Journal of Geo-Information* 4, 2842-2889.

Biljecki, F., Ledoux, H. and Stoter, J., 2016. An improved LOD specification for 3D building models. *Computers, Environment and Urban Systems*, 59, pp.25-37.

Bosch, M., Locatelli, M., Hamel, P., Remme, R. P., Chenal, J., and Joost, S. 2021. A spatially-explicit approach to simulate urban heat mitigation with InVEST (v3.8.0). *Geoscientific Model Development*, 14(6).

Buyukdemircioglu, M., Can, R., Kocaman, S., and Kada, M., 2022. Deep learning based building footprint extraction from very high resolution true orthophotos and nDSM. *ISPRS Ann. Photogramm. Remote Sens. Spatial Inf. Sci.,* V-2-2022.

Carr, J. C. and Slyder, J. B., 2018. Individual tree segmentation from a leaf-off photogrammetric point cloud. *International Journal of Remote Sensing*, *39*(15-16), 5195–5210.

Chebbi, M.A., Rupnik, E., Pierrot-Deseilligny, M. and Lopes, P., 2023. DeepSim-Nets: Deep Similarity Networks for Stereo Image Matching. Proc. *CVPR*, pp. 2096-2104.

Darvishzadeh, R., Atzberger, C., Skidmore, A.K. and Abkar, A.A., 2009. Leaf Area Index derivation from hyperspectral vegetation indices and the red edge position. *Int. Journal of Remote Sensing*, 30(23), pp.6199-6218.

Dalponte, M., Ørka, H. O., Gobakken, T., Gianelle D., and Næsset, E., 2023. Tree species classification in boreal forests with hyperspectral data. *IEEE Trans. on Geoscience and Remote Sensing*, Vol. 51(5), 2632-2645.

Di Napoli, C., Barnard, C., Prudhomme, C., Cloke, H.L., Pappenberger, F., 2020. Thermal comfort indices derived from ERA5 reanalysis. *Copernicus Climate Change Service (C3S) Climate Data Store (CDS)*.

Ellena, M., Melis, G., Zengarini, Di Gangi, E., Ricciardi, G., Mercogliano, P., Costa, G., 2023. Micro-scale UHI risk assessment on the heat-health nexus within cities by looking at socio-economic factors and built environment characteristics: The Turin case study (Italy). *Urban Climate*, Vol. 49.

Ermida, S.L., Soares, P., Mantas, V., Göttsche, F.-M., Trigo, I.F., 2020. Google Earth Engine open-source code for Land Surface Temperature estimation from the Landsat series. Remote Sensing, 12 (9), 1471.

Foshag, K., Aeschbach, N., Höfle, B., Winkler, R., Siegmund, A. & Aeschbach, W., 2020. Viability of public spaces in cities under increasing heat: A transdisciplinary approach. *Sustainable Cities and Society*, Vol. 59, pp. 102215.

Gago, E.J., Roldan, J., Pacheco-Torres, R., Ordóñez, J., 2013. The city and urban heat islands: A review of strategies to mitigate adverse effects. *Renewable and Sustainable Energy Reviews*, Vol. 25, pp. 749-758.

Garcia-Moreno, L.M., Diaz-Paz, J.P., Loaiza-Correa, H., Restrepo-Giron, A., 2020. Dataset of thermal and visible aerial images for multi-modal and multi-spectral image registration and fusion. *Data in Brief*, Vol. 29, 105326.

Gerhards, M., Schlerf, M., Rascher, U., Udelhoven, T., Juszczak, R., Alberti, G., Miglietta, F. and Inoue, Y., 2018. Analysis of airborne optical and thermal imagery for detection of water stress symptoms. *Remote Sensing*, 10(7), p.1139.

Giannelli, D., León-Sánchez, C., Agugiaro, G., 2022. Comparison and evaluation of different GIS software tools to estimate solar irradiation. *ISPRS Ann. Photogramm. Remote Sens. Spatial Inf. Sci.*, V-4-2022, pp. 285-282.

Grilli, E., Daniele, A., Bassier, M., Remondino, F., Serafini, L., 2023. Knowledge Enhanced Neural Networks for Point Cloud Semantic Segmentation. *Remote Sensing*, 15, 2590.

Grilli, E., Remondino, F., 2020. Machine Learning Generalisation across Different 3D Architectural Heritage. *ISPRS Int. J. Geo-Inf.*, 9, 379.

Gutierrez David, M., Dietrich, M., Raczko, N., Denvil, S., Santoro, M., Chatzikyriakou, C., Borejko, W., 2023. Towards the European Green Deal Data Space. Proc. *EGU General Assembly*, EGU23-8788.

Heiden, U., Heldensa, W., Roessnerb, S., Seglb, K., Escha T., and Muellera, A., 2012. Urban structure type characterization using hyperspectral remote sensing and height information. *Landscape and Urban Planning,* 105, 361– 375.

Hofierka, J. and Suri, M., 2002. The solar radiation model for Open source GIS: implementation and applications. Proc. *Open source GIS-GRASS users conference*, pp. 51-70.

Hong, D., Hu, J., Yao, J., Chanussot, J., and Zhu, X. X., 2021. Multimodal remote sensing benchmark datasets for land cover classification with a shared and specific feature learning model. *ISPRS Journal of Photogrammetry and Remote Sensing,* 178, 68–80.

Huang, J., Stoter, J., Peters, R. and Nan, L., 2022. City3D: Large-scale building reconstruction from airborne LiDAR point clouds. *Remote Sensing*, 14(9), p.2254.

Hu, J., Liu, R., Hong, D., Camero, A., Yao, J., Schneider, M., Kurz, F., Segl, K., and Zhu, X. X., 2023. MDAS: a new multimodal benchmark dataset for remote sensing. *Earth Syst. Sci. Data*, 15, 113-131.

Hyyppä, E., Kukko, A., Kaartinen, H., Yu, X., Muhojoki, J., Hakala, T., & Hyyppä, J., 2022. Direct and automatic measurements of stem curve and volume using a high-resolution airborne laser scanning system. *Science of Remote Sensing*, 5.

Kölle, M., Laupheimer, D., Schmohl, S., Haala, N., Rottensteiner, F., Wegner, J.D., Ledoux, H., 2021. The Hessigheim 3D (H3D) benchmark on semantic segmentation of high-resolution 3D point clouds and textured meshes from UAV LiDAR and Multi-View-Stereo. *ISPRS Open Journal of Photogrammetry and Remote Sensing*, 1, 100001.

Lafarge, F., Mallet, C., 2012. Creating Large-Scale City Models From 3D-Point Clouds: A Robust Approach with Hybrid Representation. *International Journal of Computer Vision* 99, 6985.

Lelégard, L., Le Bris, A. and Giordano, S., 2022. Improving Local Adaptive Filtering Method Employed in Radiometric Correction of Analogue Airborne Campaigns. *ISPRS Int. Arch. Photogramm. Remote Sens. Spatial Inf. Sci*., 43, pp.1217-1222.

Liang, J., Li, P., Zhao, H., Han, L., & Qu, M. (2020). Forest Species Classification of UAV Hyperspectral Image Using Deep Learning. *Proc. CAC, pp. 7*126-7130.

Liu, J., Gao, J., Ji, S., Zeng, C., Zhang, S., Gong, J., 2023. Deep learning based multi-view stereo matching and 3D scene reconstruction from oblique aerial images. *ISPRS Journal of Photogrammetry and Remote Sensing*, 204, pp. 42-60.

Minaee, S., Boykov, Y., Porikli, F., Plaza, A.J., Kehtarnavaz, N., Terzopoulos, D., 2021. Image segmentation using deep learning: A survey. *IEEE TPAMI*.

Moe, K., Toschi, I., Poli, D., Lago, F., Schreiner, C., Legat, K. and Remondino, F., 2016. Changing the Production Pipeline - Use of Oblique Aerial Cameras for Mapping Purposes. *ISPRS Int. Arch. Photogramm. Remote Sens. Spatial Inf. Sci*., Vol. XLI-B4, pp. 631-637.

Nex, F., Remondino, F., Agugiaro, G., De Filippi, R., Poletti, M., Furlanello, C., Menegon, S., Dallago, G., Fontanari, S., 2013. 3D SolarWeb: a solar cadaster in the Italian alpine landscape. *ISPRS Int. Arch. Photogramm. Remote Sens. Spatial Inf. Sci*., Vol. 40(7/W2).

Nowacka, A., Remondino, F., 2018. Geospatial data for energy and low carbon cities - overview, experiences and new perspectives. *ISPRS Int. Arch. Photogramm. Remote Sens. Spatial Inf. Sci.,* Vol. XLII-4.

Özdemir, E., Remondino, F., 2018. Segmentation of 3D photogrammetric point cloud for 3D building modeling. *ISPRS Int. Arch. Photogramm. Remote Sens. Spatial Inf. Sci.*, Vol. XLII-4/W10, pp. 135-142.

Özdemir, E., Toschi, I., Remondino, F., 2019. A multi-purpose benchmark for photogrammetric urban 3D reconstruction in a controlled environment. *ISPRS Int. Arch. Photogramm. Remote Sens. Spatial Inf. Sci*., Vol. XLII-1/W2, pp. 53-60.

Özdemir, E., Remondino, F., Golkar, A., 2021. An efficient and general framework for aerial point cloud classification in urban scenarios. *Remote Sensing*, 13, 1985.

Remondino, F., Morelli, L., Stathopoulou, E., Elhashash, M., Qin, R., 2022: Aerial triangulation with learning-based tie points. *ISPRS Int. Arch. Photogramm. Remote Sens. Spatial Inf. Sci.*, XLIII-B2-2022, 77-84.

Remondino, F., Karami, A., Yan, Z., Mazzacca, G., Rigon, S., Qin, R., 2023. A critical analysis of NeRF-based 3D reconstruction. *Remote Sensing*, 15, 3585.

Rottensteiner, F., Sohn, G., Jung, J., Gerke, M., Baillard, C., Benitez, S., and Breitkopf, U., 2012. The ISPRS benchmark on urban object classification and 3D building reconstruction. *ISPRS Ann. Photogramm. Remote Sens. Spatial Inf. Sci*., I-3, pp. 293-298.

Rüegg, 2019. Simultaneous heatwaves caused by anthropogenic climate change. *PhysORG*, 3.

Ruiz de Oña, E., Barbero-García, I., González-Aguilera, D., Remondino, F., Rodríguez-Gonzálvez, P., Hernández-López, D., 2023. PhotoMatch: An Open-Source Tool for Multi-View and Multi-Modal Feature-Based Image Matching. *Applied Sciences*, 13(9):5467.

Rupnik, E., Nex, F. and Remondino, F., 2014, February. Oblique multi-camera systems-orientation and dense matching issues. In *EuroCOW*

Shi, Y., Qi, Z., Liu, X., Niu, N., Zhang, H., 2019. Urban Land Use and Land Cover Classification Using Multisource Remote Sensing Images and Social Media Data. *Remote Sensing*, 11, 2719

Stathopoulou, E.K., Remondino, F., 2023. A survey of conventional and learning-based methods for multi-view stereo. *The Photogrammetric Record*, DOI: 10.1111/phor.12456

Sun, G., Jiao, Z., Li, F., Fu, H., Li, Z., 2021. Hyperspectral image-based vegetation index (HSVI): A new vegetation index for urban ecological research. *Int. Journal of Applied Earth Observation and Geoinformation*, Vol. 103, 102529.

Tian, W., Tang, L., Chen, Y., Li, Z., Qiu, S., Li, X., Hyyppä, J., 2022. Plant Species Classification Using Hyperspectral LiDAR with Convolutional Neural Network. Proc. *IGARSS,* pp. 1740-1743.

Toschi, I, Farella, E.M., Welponer, M., Remondino, F., 2021. Quality-based registration refinement of airborne LiDAR and photogrammetric point clouds. *ISPRS Journal of Photogrammetry and Remote Sensing*, Vol. 172, pp. 160-170.

Toschi, I., Nocerino, E., Remondino, F., Revolti, A., Soria, G., Piffer, S., 2017. Geospatial data processing for 3D city model generation, management and visualization. *ISPRS Int. Arch. Photogramm. Remote Sens. Spatial Inf. Sci.,* Vol. XLII-1-W1, pp. 527-534.

Turki, H., Ramanan, D., Satyanarayanan, M., 2022. Mega-NeRF: scalable construction of large-scale NeRFs for virtual fly-throughs. Proc. *CVPR.*

Voelkel, J., Shandas, V., 2017. Towards systematic prediction of urban heat islands: grounding measurements, assessing modeling techniques. *Climate*, Vol. 5(2).

Xia, G.-S., Hu, J., Hu, F., Shi, B., Bai, X., Zhong, Y., Zhang, L., and Lu, X., 2017. AID: A benchmark data set for performance evaluation of aerial scene classification, *IEEE T. Geosci. Remote*, 55, 3965–3981.

Wouters, H., De Ridder, K., Poelmans, L., Willems, P., Brouwers, J., Hosseinzadehtalaei, P., Tabari, H., Vannden Broucke, S., van Lipzig, N.P.M., Demuzere, M., 2017. Heat stress increase under climate change twice as large in cities as in rural areas: A study for a densely populated midlatitude maritime region. *Geophysical Research Letters*, 44 (17).

Wu, G., Shao, X., Guo, Z., Chen, Q., Yuan, W., Shi, X., Xu, Y., Shibasaki, R., 2018. Automatic building segmentation of aerial imagery using multi-constraint fully convolutional networks. *Remote Sensing*, 10(3):407.

Zhao, H., Jiang, L., Jia, J., Torr, P.H. and Koltun, V., 2021. Point transformer. Proc. *ICCV*, pp. 16259-16268.